Kaiser et al Congenital

Simulation-based design of bicuspidization of the aortic valve

Alexander D. Kaiser, PhD, a,b Moussa A. Haidar, MD, Perry S. Choi, MD, Amit Sharir, BS, Alison L. Marsden, PhD, a,b,d,e and Michael R. Ma, MD,c

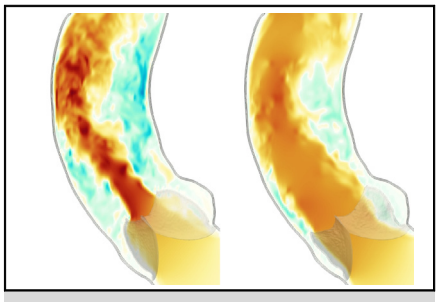
ABSTRACT

Objective: Severe congenital aortic valve pathology in the growing patient remains a challenging clinical scenario. Bicuspidization of the diseased aortic valve has proven to be a promising repair technique with acceptable durability. However, most understanding of the procedure is empirical and retrospective. This work seeks to design the optimal gross morphology associated with surgical bicuspidization with simulations based on the hypothesis that modifications to the free edge length cause or relieve stenosis.

Methods: Model bicuspid valves were constructed with varying free edge lengths and gross morphology. Fluid-structure interaction simulations were conducted in a single patient-specific model geometry. The models were evaluated for primary targets of stenosis and regurgitation. Secondary targets were assessed and included qualitative hemodynamics, geometric height, effective height, orifice area, and billow.

Results: Stenosis decreased with increasing free edge length and was pronounced with free edge length less than or equal to 1.3 times the annular diameter *d*. With free edge length 1.5*d* or greater, no stenosis occurred. All models were free of regurgitation. Substantial billow occurred with free edge length 1.7*d* or greater.

Conclusions: Free edge length 1.5*d* or greater was required to avoid aortic stenosis in simulations. Cases with free edge length 1.7*d* or greater showed excessive billow and other changes in gross morphology. Cases with free edge length 1.5*d* to 1.6*d* have a total free edge length approximately equal to the annular circumference and appeared optimal. These effects should be studied in vitro and in animal studies. (J Thorac Cardiovasc Surg 2024; ■:1-10)



In simulations of bicuspidization repair, increasing free edge length reduced stenosis.

CENTRAL MESSAGE

Simulations suggest that total free edge length approximately equal to the annular circumference reduces stenosis in bicuspidization of the aortic valve.

PERSPECTIVE

Bicuspidization of the aortic valve is an effective repair strategy for severe congenital aortic valve pathology. Despite positive outcomes, postoperative stenosis is common. Systematically conducted computer simulations showed that a free edge length of 1.5 to 1.6 times the annular diameter reduced stenosis. Surgeons should consider increasing free edge length to reduce stenosis and improve outcomes.

See Commentary on page XXX.

Severe congenital aortic valve pathology in the growing patient remains a challenging clinical scenario, with dysplastic morphology often too complex for common repair strategies and size too small for durable prosthetic options. Over the years, this dilemma has pushed surgeons

to devise numerous creative attempts at a durable surgical solution. First conceived by Schäfers and colleagues, one of these surgical approaches involves bicuspidization of the diseased aortic valve, with particular emphasis on the creation of 2 commissures of equal height. The

From the ^aDivision of Pediatric Cardiology, Department of Pediatrics, ^bCardiovascular Institute, ^cDivision of Pediatric Cardiac Surgery, Department of Cardiothoracic Surgery, ^dDepartment of Bioengineering, and ^eInstitute for Computational and Mathematical Engineering, Stanford University, Stanford, Calif.

P.S.C. was funded in part by a grant from the National Institutes of Health #R38HL143615.

Institutional Review Board (IRB) number and approval date: #39377, June 27, 2023. The IRB of the Stanford University approved the study protocol and publication of data. Patient written consent for the publication of the study data was waived by the IRB for use of anonymized, retrospectively acquired data.

Received for publication Sept 22, 2023; revisions received Dec 5, 2023; accepted for publication Dec 21, 2023.

Address for reprints: Michael R. Ma, MD, Department of Cardiothoracic Surgery, Stanford University, Falk Building, CVRB, 300 Pasteur Dr, Stanford, CA 94305 (E-mail: mma@stanford.edu).

0022-5223/\$36.00

Copyright © 2024 by The American Association for Thoracic Surgery https://doi.org/10.1016/j.jtcvs.2023.12.027 Congenital Kaiser et al

Abbreviations and Acronyms

d = annular diameter E_h = effective height

 $E_{h,min} = \text{effective height from minimum height of}$

valve taking billow into account

F = free edge length G_h = geometric height r = annular radius STJ = sinotubular junction



Scanning this QR code will take you to the table of contents to access supplementary information.

reconstructed valve resembles a Sievers type 0 pure bicuspid valve.² Although originally conceived for unicuspid aortic valve disease—with 1 fully developed commissure of normal height and 2 other commissures with rudimentary raphae and lower height—the technique has since been applied in other lesions, such as bicuspid, tricuspid, and quadricuspid variants.³ Despite overall promising results, postoperative stenosis is common, with some studies citing moderate or greater stenosis (>20 mm Hg) in up to 75% of patients. 1,3 Further, design principles based on engineering analysis are largely unknown regarding this repair. In this work, simulation-based design tools to optimize the gross morphology of the pure bicuspid aortic valve were developed. The objective was to find a gross morphology that was free of stenosis and regurgitation and to create straightforward guidelines that can be tested in future benchtop and animal studies and translated to clinical practice.

The optimal geometry of a pure bicuspid valve appears to be largely unexplored, but related studies have investigated the performance of native bicuspid valves and the typical configuration of a normal trileaflet aortic valve. One study found a rare porcine specimen of a pure bicuspid valve and studied its hemodynamics ex vivo.4 Most modeling studies on bicuspid valves have focused on Sievers type 1 bicuspid valve with a raphe. Emendi and colleagues⁵ investigated the hemodynamics of bicuspid valves in a patientspecific case and compared them with clinical imaging. We simulated multiple fusion locations in a single patientspecific geometry and showed that hemodynamics were highly dependent on valve phenotype.⁶ Lavon and colleagues⁷ studied the effects of cusp angles, and Rego and colleagues⁸ modeled strain in patient-specific models including the valve only without fluid. In contrast to the pure bicuspid case, there is substantial literature on the native, presumably optimal, geometry of the healthy trileaflet valve. 9-11 In a previous modeling study, we found that the trileaflet aortic valve was highly sensitive to changes in gross morphology. 12

In our previous work, methods were developed to construct model valves from as close as possible to first principles ^{12,13} and used to conduct a controlled comparison of flows associated with different valve phenotypes. ⁶ A benchtop experiment of flow through a prosthetic valve was conducted and imaged with 4-dimensional flow magnetic resonance imaging. Modeling this experiment and conducting a detailed comparison between experimental and simulation data revealed excellent qualitative and reasonable quantitative agreement between them. ¹⁴ Thus, our methods are reliable for simulating realistic flow through heart valves. Simulations using related patient-specific modeling methods have been applied to model complex congenital heart disease and impacted clinical practice. ^{15,16}

In this work, models of the pure bicuspid aortic valve were created and studied with fluid-structure interaction simulations. With fluid-structure interaction simulations, a system of partial differential equations representing the coupled dynamics of the valve and blood was solved to produce detailed predictions of blood velocity and leaflet motion throughout the cardiac cycle. Valve performance was evaluated for stenosis, regurgitation, and diastolic gross morphology. We believe this is the first study to simulate flow through the pure bicuspid valve and use simulation-based design for bicuspidization of the aortic valve.

MATERIALS AND METHODS

Simulation Methods

The model valves were constructed, as nearly as possible, from first principles via a process referred to as "design-based elasticity." 12,13 Via the requirement that tension in the leaflets must support a pressure load, an associated system of partial differential equations was derived representing the mechanical equilibrium of the leaflets under pressure. The solution to these equations represented the loaded, closed configuration of the valve. Parameters were tuned in this elasticity problem to design the gross morphology and material properties of the models. Because the valve models were derived from nearly first principles, the emergent material properties mimicked those of native tissue and produced effective valve closure in simulations.

By using this process, 8 model bicuspid valves were constructed, composed of 2 equally sized leaflets and 2 commissures of equal height 180 degrees apart. The planar circle at the base of the annulus was referred to as the "virtual basal ring." In this study, the diameter of the entire 3 dimensional annulus was kept constant at d=25 mm from the virtual basal ring to the sinotubular junction (STJ), including the intercommissural distance. The free edge length at rest varied from approximately 1.1d to 1.8d in increments of 0.1d. The model at approximately 1.6d had, more precisely, free edge length of 1.57d, so both free edge lengths added up to approximately πd , or the circumference of the annulus. As the free edge length increased in the design-based model construction, additional length

Kaiser et al Congenital

was added accordingly to the circumferential (commissure to commissure) curves throughout the leaflet, adding area overall to the leaflet including the leaflet belly. An additional set of models were constructed that all have free edge length of approximately 1.6d with less leaflet area or "bowl" in the leaflet belly, less leaflet height, and both less bowl and height (Appendix E1 and Figure E1). The leaflets were attached to a rigid scaffold that supported the valve at both commissures. The diameter of the scaffold was constant throughout the annulus from the virtual basal ring to the STJ, which forced the intercommissural distance to be equal to the annular diameter. One commissure was aligned with the patient's left coronary and noncoronary commissure, because this commissure is most frequently normal in patients with a unicuspid valve and left in position.^{2,3} The opposing commissure was supported by the scaffold, which covered any residual space between the valve and sinus.

A patient-specific model aorta geometry was constructed in which to mount the model valves. An anonymized computed tomography scan of a patient with no known aortic or valvular disease was retrospectively acquired. The Institutional Review Board of the Stanford University approved the study protocol and publication of data. Patient written consent for the publication of the study data was waived by the Institutional Review Board for use of anonymized, retrospectively acquired data (#39377, June 27 2023). The aortic geometry was manually segmented from this computed tomography scan using SimVascular. This patient had approximately equal diameter of the aortic annulus from the virtual basal ring to the STJ.

Fluid-structure interaction simulations were performed with the immersed boundary method, a numerical method that is well suited to simulations involving heart valves, ^{19,20} using the open-source solver Immersed Boundary Adaptive Mesh Refinement (IBAMR).²¹ Simulations were driven by prescribing pressures at the inlet, approximately at the left ventricular outflow tract, and the outlet, in the distal ascending aorta. More details are described in the Appendix E1.

Evaluation Metrics

Scalar metrics were computed to evaluate valve performance. In systole, the orifice area of the open valve, the mean pressure gradient in mid systole, and the stroke volume were computed. In diastole, metrics were computed based on gross morphology (Figure 1). The geometric height G_h represented the 3-dimensional length of the midline curve of the leaflet from annulus to free edge. The quantity G_h/r was the geometric height normalized to the radius of the annulus. The billow height measured the lowest point of the leaflet in the direction normal to the virtual basal ring; if this quantity was positive, there was no billow. The effective height E_h measured the distance from the virtual basal ring in the normal direction to the center of the free edge of the leaflet. The effective height measured from the minimum height of the valve was denoted $E_{h,min}$ and takes billow into account. The quantities E_h/G_h , $E_{h,min}/G_h$ represented the ratio of effective height over geometric height and the ratio of effective height considering billow over geometric height. The free edge length F represented

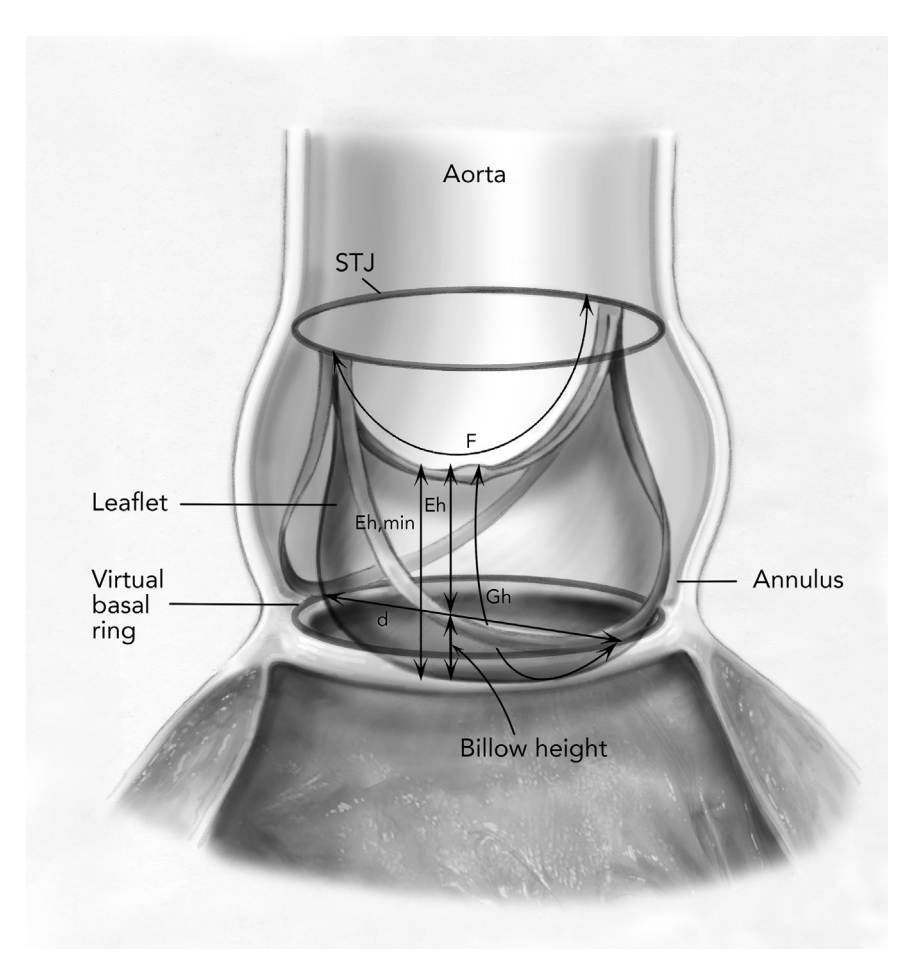


FIGURE 1. Schematic showing gross morphology. STJ, Sinotubular junction; E_h , effective height; $E_{h,min}$, effective height from minimum considering billow height; G_h , geometric height; d, annular diameter.

Congenital Kaiser et al

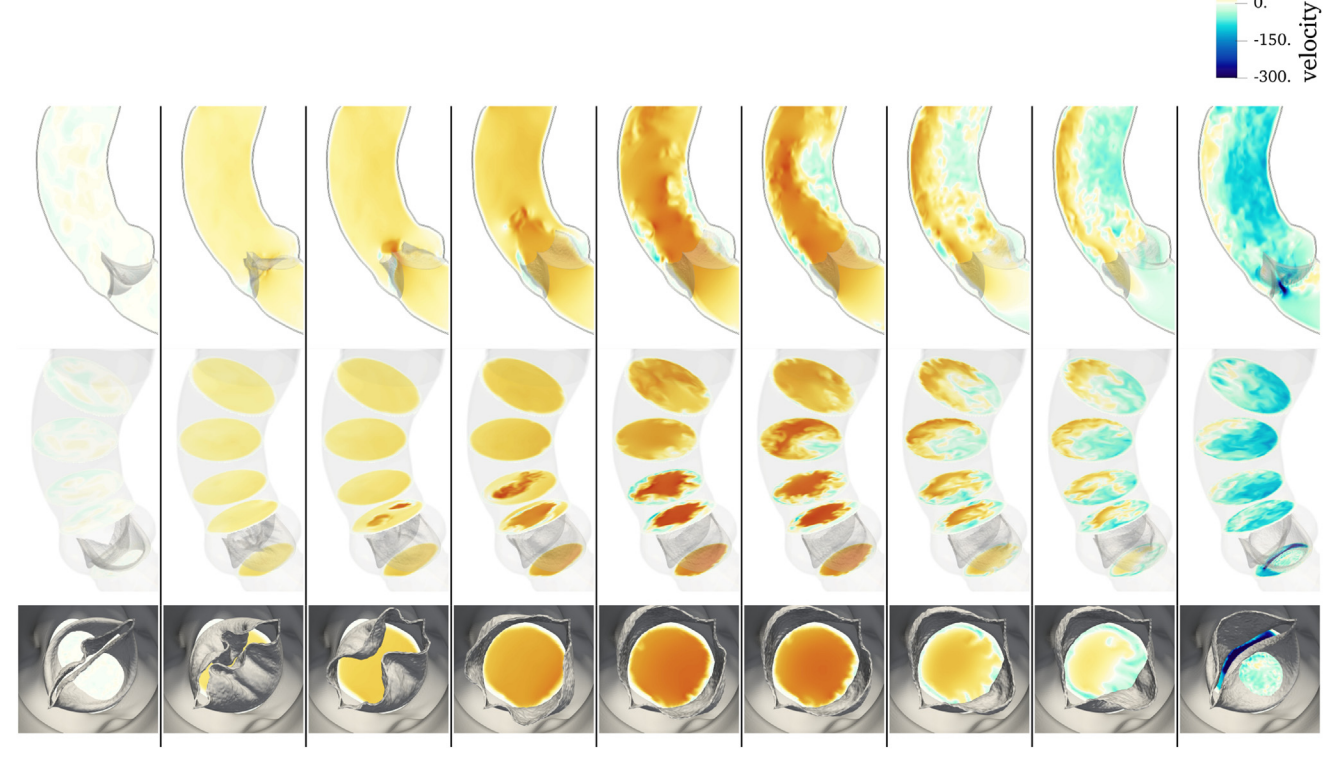


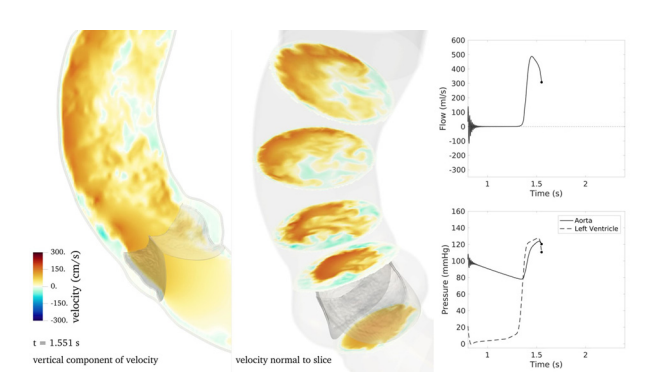
FIGURE 2. Flows through the cardiac cycle, 1.57*d* case.

the 3-dimensional length of the leaflet as it runs from commissure to commissure, which was computed on the aortic side of the free edge. The quantity F/d represented the free edge length normalized by the valve diameter.

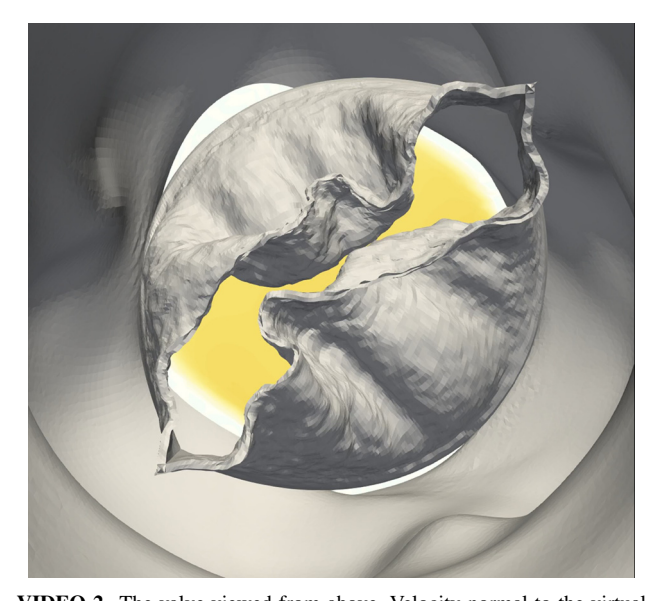
increasing stenosis with decreasing free edge length. The 1.4d case showed marginally higher pressure gradient than the larger cases. The cases with free edge rest lengths

RESULTS

Fluid-structure interaction simulations were performed on cases with varying free edge lengths. Cases with free edge rest length 1.5d or greater were free of any stenosis. Cases with free edge rest length 1.3d or less showed



VIDEO 1. Slice views of fluid velocity plus driving pressures and flow rate. Each free edge length was approximately 1.57 times the annular diameter. Video available at: https://www.jtcvs.org/article/S0022-5223(24) 00009-6/fulltext.



VIDEO 2. The valve viewed from above. Velocity normal to the virtual basal ring is shown. Each free edge length was approximately 1.57 times the annular diameter. Video available at: https://www.jtcvs.org/article/S0022-5223(24)00009-6/fulltext.

Kaiser et al Congenital

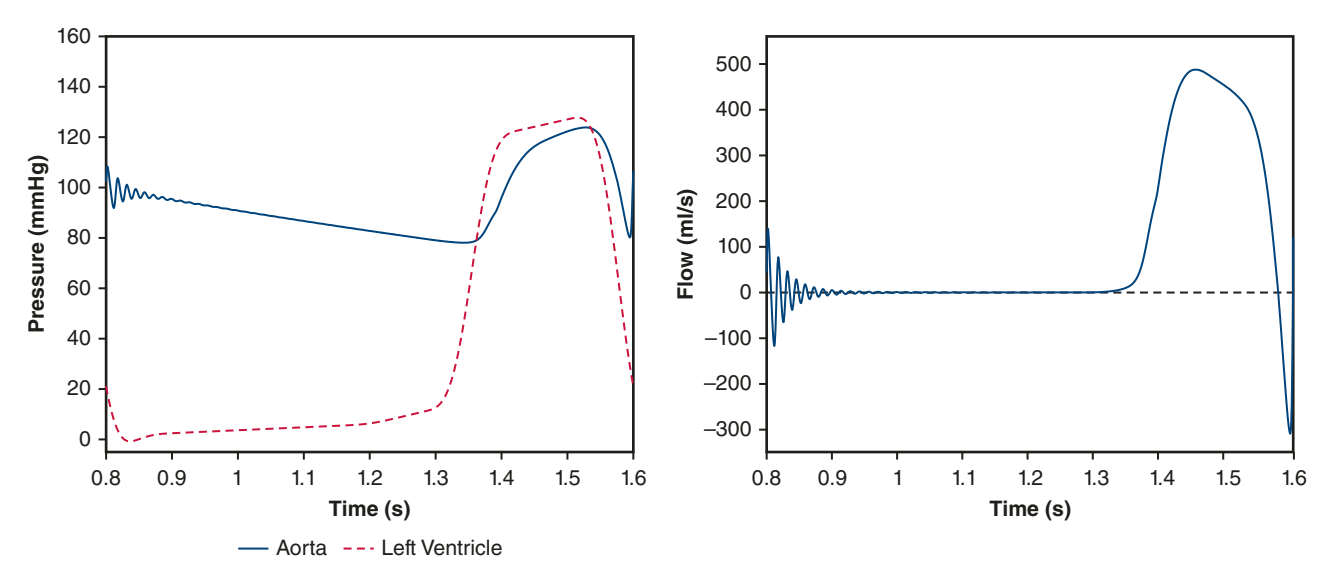


FIGURE 3. Pressure and flow waveforms on the 1.57d case from the second cardiac cycle.

1.7d or greater showed good systolic performance, but excessive billow during diastole.

The dynamics of blood velocity and valve motion on the 1.57d case through the cardiac cycle appeared qualitatively excellent, with no apparent stenosis or regurgitation (Figure 2; Videos 1 and 2). The top row shows the vertical component of velocity on a slice through the center of the virtual basal ring. The middle row shows the axial component of velocity on 5 slices that are approximately normal to the axis of the vessel. The slices are located at the virtual basal ring, the STJ, and the bottom, middle, and distal portions of the ascending aorta. The bottom row shows the valve from above along with the velocity normal to the virtual basal ring. If the leaflets billowed, the velocity at the virtual basal ring appeared above the leaflets in the visualization, serving as a visual queue for billow.

The pressure and flow waveforms during the second cardiac cycle on the 1.57*d* case suggested the valve was free of dysfunction (Figure 3). The flow rate showed an oscillation that rapidly decayed in amplitude, remained nearly zero through diastole, and then increased rapidly in systole. The waveforms indicated that under physiological pressures, the valve opens freely and closes reliably.

The blood velocity and valve position in mid-systole varied substantially across cases (Figure 4). The cases with shorter free edge lengths showed stenosis via a visibly narrowed valve orifice and jet of forward flow. The 1.1d case appeared highly stenotic, with a large fraction of the orifice obstructed by the leaflets. At the STJ, the narrowed jet of forward flow was surrounded by relatively static flow. Just above, regions of backflow surrounded the jet. In the distal ascending aorta, the jet impacted the greater curvature of the vessel, and a region of reverse flow was apparent on

the inner side or lesser curvature. The narrowed jet thus caused local regions of retrograde flow. The 1.2d case showed similar features to the 1.1d case but was modestly less stenotic with a slightly wider jet. The 1.3d case was similar to the 1.2d case and was omitted for clarity. The 1.4d case showed a subtly narrower jet of forward flow and larger areas of backflow than the cases with more free edge rest length.

The cases with more free edge length showed uninhibited forward flow and no apparent stenosis. The 1.57d case, which has a free edge rest length approximately equal to the circumference of the annulus, showed a wide opening and jet of forward flow and negligible backflow. The 1.5d case appeared nearly identical to the 1.57d case and was omitted. The 1.8d case had similar unrestricted forward flow to the 1.57d case but appeared to have "excess" leaflet material in the sinus, with rippling or bunching of the leaflets visible. The 1.7d case showed similar excess material and was omitted.

Billow increased with increasing free edge length in middiastole (Figure 5). In all cases, there was no visible regurgitation. The distal ascending aorta and middle panel were omitted, because blood velocity is nearly zero. In the 1.1dcase, the top view showed a fairly straight line of coaptation and small regions of billow on each leaflet belly. On the 1.2dcase, the free edge showed a subtly larger region of billow. The 1.4d case showed more redundancy on the free edge length, with a slight ripple forming. In the 1.57d case, the leaflets were visible below the virtual basal ring, and a portion of the leaflet belly dipped below the ring. On 1 leaflet, a small fold of redundant material was present on the free edge. In the 1.8d case, the majority of the leaflet belly billowed below the virtual basal ring. Even the center Congenital Kaiser et al

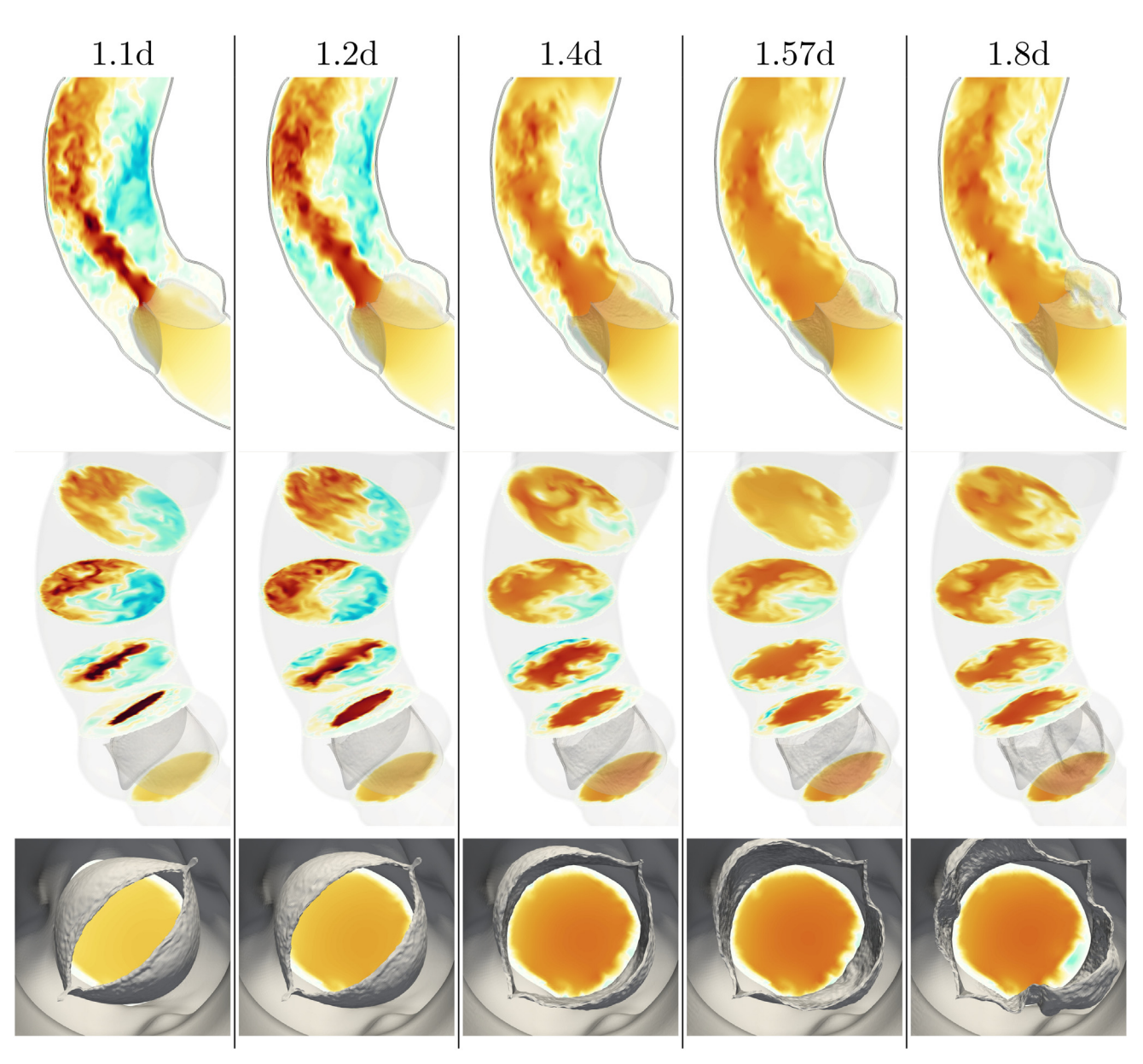


FIGURE 4. Flows in mid systole. The cases with free edge rest lengths of 1.1d and 1.2d showed obvious stenosis, reduced orifice area, and narrowed jets of forward flow. The case with free edge rest length 1.4d had considerably less restriction; the cases with 1.57d and 1.8d had no apparent stenosis or restriction to forward flow. d. Annular diameter.

of the free edge dipped slightly below the plane of the virtual basal ring, making for a negative effective height. The 1.3d, 1.5d, and 1.7d cases were similar to the cases of comparable free edge lengths and omitted.

The pressure gradient decreased, and flow rate increased monotonically with increasing free edge length up to 1.5d, above which there was little difference in pressure and flow rate (Figure 6). The 1.1d case was highly stenotic, with a sustained pressure gradient over 30 mm Hg and a correspondingly low flow rate. The 1.2d case was also stenotic, with peak pressure gradient of over 20 mm Hg. The 1.3d case showed a slightly lower pressure gradient and modest

loss of flow rate. The 1.4d case showed a subtly higher pressure gradient and lower flow rate than subsequent cases, indicating there was still insufficient free edge length to minimize the pressure gradient. The 1.5d to 1.8d cases all showed similar pressure gradients and flow rates, indicating that the free edge length was sufficient to open widely and leave the annulus free of obstruction.

Scalar metrics varied widely in both systole and diastole across cases (Table 1). The geometric heights and nondimensional geometric heights were relatively consistent throughout the models, by design. The billow height increased monotonically with free edge length, with

Kaiser et al Congenital

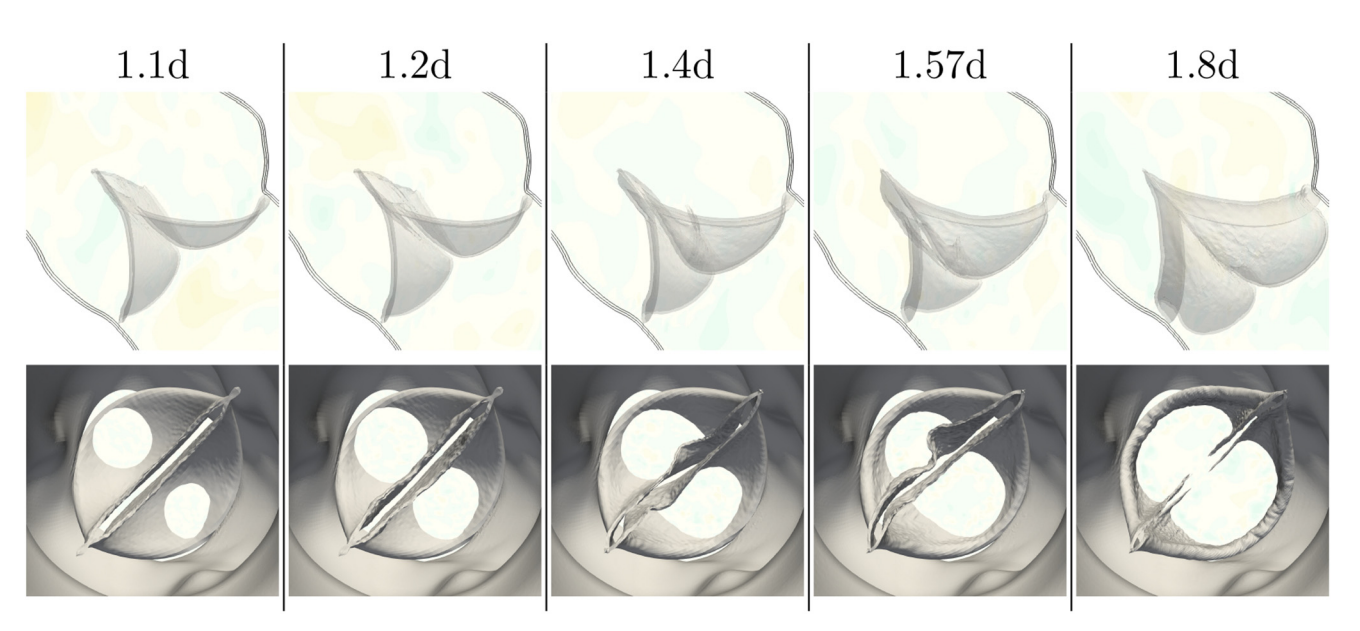


FIGURE 5. Flows in diastole. The valves were sealed with no regurgitation visible in all cases. Billow increased with increasing free edge length. d, Annular diameter.

substantial billow on the 1.7d and 1.8d cases. The effective height varied widely, from greater than 1.1 cm to less than 0 cm, meaning that part of the free edge in the most billowed case was below the virtual basal ring. The effective height from minimum decreased similarly but was, by definition, larger. The effective height to geometric height ratio was 0.5 in the 1.1d case, approximately 0.3 for the 1.4d to 1.57dcases, and approximately zero for the most billowed cases. Taking billow into account, the ratio $E_{h,min}/G_h$ was 0.39 or greater for the 1.1 to 1.57 cases, but less than 0.3 in the 1.7d and 1.8d cases. The nondimensional free edge length F/d in all cases was slightly larger than the free edge rest length for each case, as expected because the free edge was loaded. In systole, the orifice area increased, the pressure gradient decreased, and the stroke volume increased with increasing free edge length up to the 1.4d case. The 1.5d to 1.8d cases showed approximately constant area, pressure gradient, and stroke volume. This behavior suggested that adding additional free edge rest length beyond 1.5d had little effect on the systolic performance of the valve.

Models with consistent free edge length and altered gross morphology are discussed in the Appendix E1.

DISCUSSION

Fluid-structure interaction simulations were conducted to optimize the gross morphology of bicuspidization of the aortic valve. Configurations with free edge rest length 1.3 times the annular diameter or less showed clinically relevant stenosis with mean pressure gradients exceeding 12 mm Hg. Cases with free edge rest length 1.5 times the

diameter or greater showed sustained pressure gradients below 8 mm Hg. Increasing the free edge length further did not reduce this gradient. The case with free edge rest length 1.4 times the diameter had a slightly higher pressure gradient than the cases with free edge rest length 1.5 times the diameter or greater. Configurations that avoided stenosis had free edge lengths that were relatively large, meaning the leaflets also had large surface area. This large surface area led to leaflet billow and decreased effective height, although without apparent regurgitation.

On the basis of these results, we propose that free edge rest length of approximately 1.57d on each leaflet is optimal for reducing stenosis. This case had no apparent stenosis and unrestricted forward flow, but less billow and excess material than cases with more free edge length.

The following calculation explains some of the challenges of constructing a bicuspid valve with 2 equal leaflets. When the closed geometry is projected onto a 2-dimensional plane, the projected total free edge length is approximately 2d. To open fully and avoid any obstruction to forward flow or stenosis, the free edge length must be approximately the same length as the circumference of the aortic annulus, or πd or just over 3d. This calculation suggests an optimal total free edge length slightly exceeding 2d in diastole, accounting for the central coaptation point being lower than the commissures. The optimal length in systole, however, is slightly larger than 3d. Further, in systole the leaflets are less loaded and thus less stretched and smaller. Therefore, additional redundant length of order d in the diastolic configuration is necessary

Congenital Kaiser et al

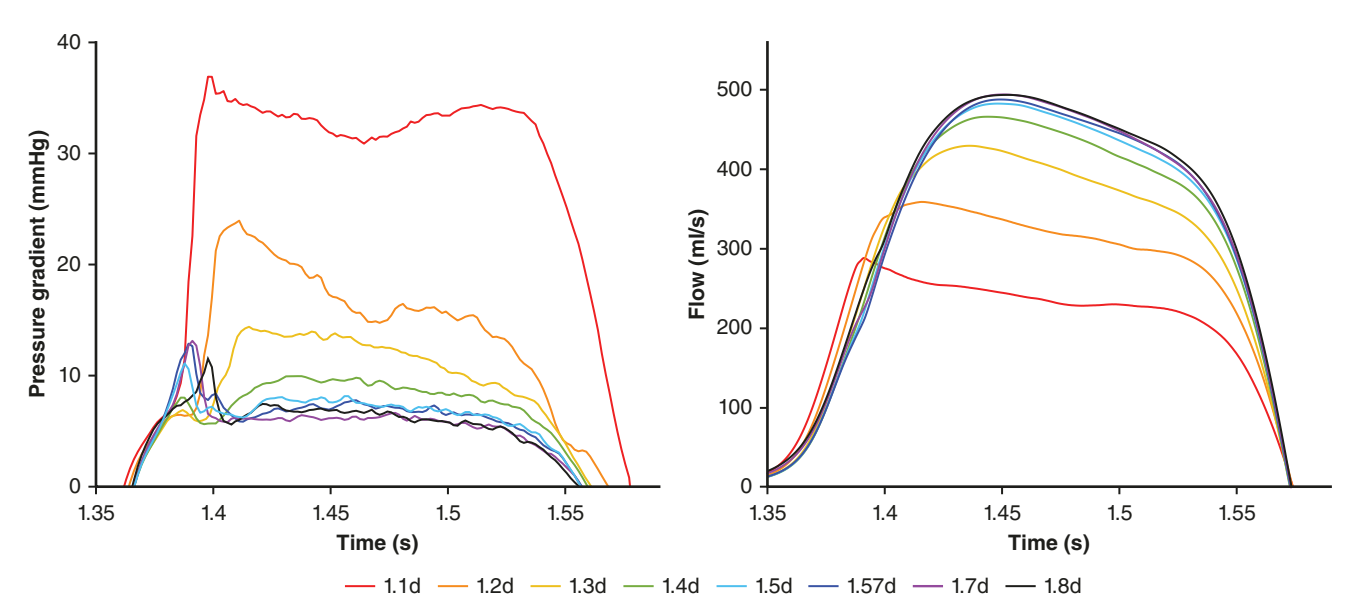


FIGURE 6. Pressure gradients and flow rates in systole compared across multiple cases. The cases with free edge length 1.3d or under showed stenosis and reduced flow. The cases with free edge length 1.5d or greater showed pressure gradients under 10 mm and similar flow rates. d, Annular diameter.

for a nonrestrictive systolic configuration. Our predicted optimal free edge length of 1.57d for each leaflet and 3.14d in total thus provides sufficient length for good opening, while showing only modest billow compared with the 1.7d and 1.8d cases.

Similar estimates for a healthy, normal trileaflet valve starkly contrast with these results. Again projecting onto a 2-dimensional plane, each leaflet has free edge length d so the total projected free edge length is 3d, and the 3-dimensional length is just over 3d. Then with a small

TABLE 1. Scalar metrics in systole and diastole

Systole						
Case	Orifice area (cm²)	Pressure gradient, mean (mm Hg)	Stroke volume (mL)			
1.1 <i>d</i>	1.31	32.94	46.36			
1.2 <i>d</i>	1.86	17.30	59.11			
1.3 <i>d</i>	2.53	12.19	67.99			
1.4 <i>d</i>	3.05	9.09	73.08			
1.5 <i>d</i>	3.37	7.37	75.10			
1.57 <i>d</i>	3.45	6.92	75.52			
1.7 <i>d</i>	3.42	6.03	77.01			
1.8 <i>d</i>	3.46	6.50	78.20			

Diastole									
Case	G_h (cm)	G_h/r (cm)	Billow height (cm)	E_h (cm)	Eh,min (cm)	Eh/Gh	Eh,min/Gh	F (cm)	F/d
1.1 <i>d</i>	2.23	1.79	-0.13	1.12	1.25	0.50	0.56	2.95	1.18
1.2 <i>d</i>	2.28	1.82	-0.20	0.97	1.17	0.42	0.51	3.12	1.25
1.3 <i>d</i>	2.26	1.81	-0.23	0.89	1.12	0.39	0.50	3.42	1.37
1.4 <i>d</i>	2.20	1.76	-0.24	0.68	0.93	0.31	0.42	3.68	1.47
1.5 <i>d</i>	2.22	1.78	-0.28	0.59	0.87	0.27	0.39	3.93	1.57
1.57 <i>d</i>	2.15	1.72	-0.28	0.59	0.87	0.27	0.40	4.02	1.61
1.7 <i>d</i>	2.22	1.78	-0.44	0.21	0.65	0.09	0.29	4.49	1.80
1.8 <i>d</i>	2.31	1.85	-0.56	-0.03	0.53	-0.01	0.23	4.84	1.94

d, Annular diameter; G_h , geometric height; r, annular radius; E_h , effective height; $E_{h,min}$, effective height from minimum height of valve taking billow into account; F, free edge length.

Kaiser et al Congenital

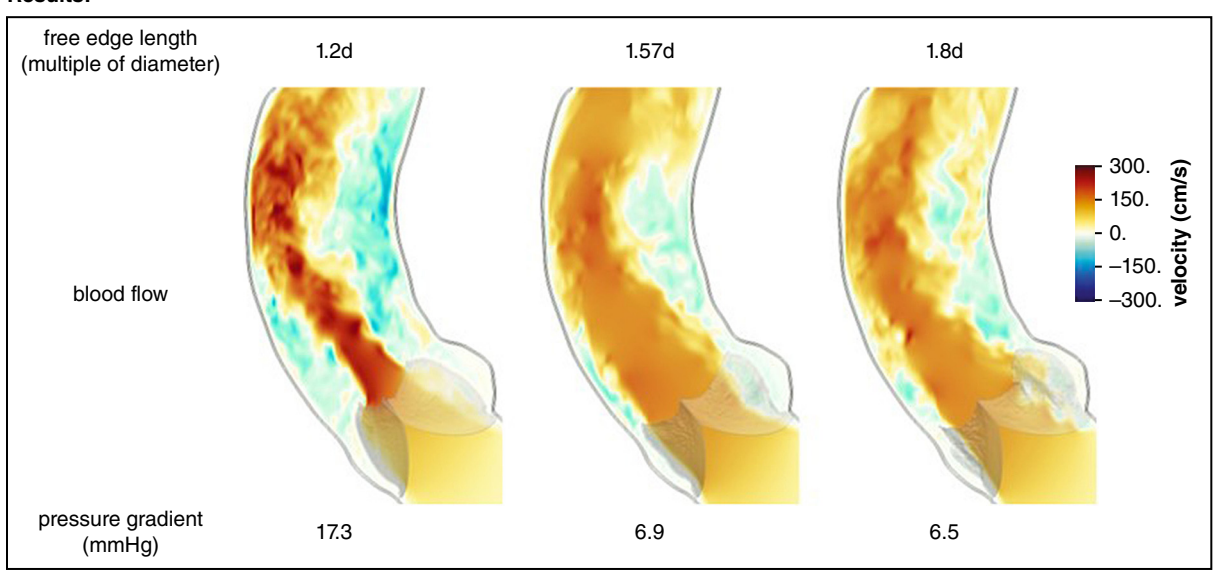
Simulation-Based Design of Bicuspidization of the Aortic Valve

Methods:

Fluid-structure interaction simulations to evaluate and reduce stenosis in bicuspidization of the aortic valve

- · One patient-specific aortic geometry
- Eight model bicuspid valves with free edge length from 1.1 to 1.8 times the annular diameter d

Results:



· Stenosis decreased with increasing free edge length.

Implications:

· Surgeons should consider increasing free edge length in bicuspidization of the aortic valve to reduce postoperative stenosis.



@AATSHQ

FIGURE 7. Summary of simulation-based design study of bicuspidization of the aortic valve. Results showed that stenosis decreased with increasing free edge length. Cases with free edge length 1.5 to 1.6 times the annular diameter showed no stenosis and appeared optimal.

relative change in length, the leaflets can deform from the closed configuration to an open configuration with free edge length approximately equal to the circumference of the annulus, which is πd or just over 3d. This suggests a much smaller relative change in leaflet lengths through the cardiac cycle is necessary with normal trileaflet anatomy.

In this study, it was assumed that the annular diameter is constant from the virtual basal ring to the STJ. In cases where the diameters differ, the STJ diameter, which is equal to the intercommissural distance, is likely the relevant diameter operatively. Because the STJ can be more easily remodeled operatively, however, using the virtual basal ring diameter and resizing the STJ accordingly may be an attractive clinical option. With a constant leaflet geometry on a trileaflet case, a modeling study showed substantial differences in coaptation with changes in the virtual basal ring diameter while keeping the STJ diameter fixed.²² Thus, a systematic comparison of optimal performance with

variations in diameter at the virtual basal ring and STJ would be highly relevant for future work.

We believe the general trends presented in this work are widely applicable to any surgeon interested in optimizing bicuspidization of the aortic valve. Further laboratory, animal, and human studies should be conducted to validate these predictions and apply them to clinical practice.

Study Limitations

A number of minor limitations were present in this study. Compensatory measures for left ventricular pressure were not considered, but if they were included, the increases in flow rate would have caused even more pressure gradient to occur in the stenotic cases. Leaflet material properties were modeled approximately as healthy native tissue, whereas surgical reconstruction would include pericardial or synthetic material. Suture lines may further influence valve kinematics. The model valves were all mounted to a stiff scaffold (like a virtual sewing ring) that rigidly held

Congenital Kaiser et al

the commissures precisely in place 180 degrees across the annulus, which may not be possible to achieve depending on the patient's anatomy.

CONCLUSIONS

Simulations showed that stenosis decreased with increasing free edge length, and that with free edge lengths 1.5 times or more the annular diameter, no stenosis occurred (Figure 7). The optimal configurations showed substantial extra, redundant leaflet material and free edge length when closed, resulting in leaflet billow and the appearance of excessive free edge length in diastole. Despite an imperfect appearance when closed, these valves functioned well, without stenosis or regurgitation. In contrast, configurations with a shorter free edge length had less billow and a straighter, more "crisp" coaptation line, but stenosis occurred during systole. These models, despite a subjectively better appearance in diastole, showed dysfunction in systole.

Although the optimal repair may depend on the individual anatomy, the general trend predicted in this work is clear: With inadequate free edge length, bicuspid valves showed stenosis, and augmenting free edge length resolved the stenosis.

Our results suggest that surgeons should consider including additional free edge length to avoid stenosis in surgical bicuspidization of the aortic valve.

Conflict of Interest Statement

The authors reported no conflicts of interest.

The *Journal* policy requires editors and reviewers to disclose conflicts of interest and to decline handling or reviewing manuscripts for which they may have a conflict of interest. The editors and reviewers of this article have no conflicts of interest.

Figure 1 was illustrated by Michael Leonard of University of the Pacific. Computing for this project was performed on the Stanford University's Sherlock cluster with assistance from the Stanford Research Computing Center. Simulations were performed using the open-source solver package IBAMR (https://ibamr.github.io).

References

- Schäfers HJ, Aicher D, Riodionycheva S, Lindinger A, Rädle-Hurst T, Langer F, et al. Bicuspidization of the unicuspid aortic valve: a new reconstructive approach. Ann Thorac Surg. 2008;85:2012-8. https://doi.org/10.1016/j.athoracsur.2008.02.081
- Sievers HH, Schmidtke C. A classification system for the bicuspid aortic valve from 304 surgical specimens. *J Thorac Cardiovasc Surg.* 2007;133:1226-33. https://doi.org/10.1016/j.jtcvs.2007.01.039
- Chiu P, Chávez M, Zubair MM, Friedman KG, Marx GR, Del Nido PJ, et al. Symmetric bicuspidizing repair for patients with congenital aortic or truncal valve

- disease. J Thorac Cardiovasc Surg. 2022;166:283-91. https://doi.org/10.1016/j.itevs.2022.10.015
- Zhu Y, Imbrie-Moore AM, Park MH, Paulsen MJ, Wang H, MacArthur JW, et al. Ex vivo analysis of a porcine bicuspid aortic valve and aneurysm disease model. Ann Thorac Surg. 2021;111:e113-5. https://doi.org/10.1016/j.athoracsur.2020. 05 086
- Emendi M, Sturla F, Ghosh RP, Bianchi M, Piatti F, Pluchinotta FR, et al. Patientspecific bicuspid aortic valve biomechanics: a magnetic resonance imaging integrated fluid–structure interaction approach. *Ann Biomed Eng.* 2021;49:627-41. https://doi.org/10.1007/s10439-020-02571-4
- Kaiser AD, Shad R, Schiavone N, Hiesinger W, Marsden AL. Controlled comparison of simulated hemodynamics across tricuspid and bicuspid aortic valves. *Ann Biomed Eng.* 2022;50:1053-72. https://doi.org/10.1007/s10439-022-02983-4
- Lavon K, Halevi R, Marom G, Ben Zekry S, Hamdan A, Joachim Schäfers H, et al. Fluid–structure interaction models of bicuspid aortic valves: the effects of nonfused cusp angles. J Biomech Eng. 2018;140:1-7. https://doi.org/10.1115/1.4038329
- Rego BV, Pouch AM, Gorman JH, Gorman RC, Sacks MS. Patient-specific quantification of normal and bicuspid aortic valve leaflet deformations from clinically derived images. *Ann Biomed Eng.* 2022;50:1-15. https://doi.org/10.1007/s10439-021-02882-0
- Swanson WM, Clark RE. Dimensions and geometric relationships of the human aortic valve as a function of pressure. Circ Res. 1974;35:871-82. https://doi.org/ 10.1161/01.RES.35.6.871
- Jelenc M, Jelenc B, Poglajen G, Lakič N. Aortic valve leaflet and root dimensions in normal tricuspid aortic valves: a computed tomography study. J Card Surg. 2022;37:2350-7. https://doi.org/10.1111/jocs.16587
- Schäfers HJ, Schmied W, Marom G, Aicher D. Cusp height in aortic valves. J Thorac Cardiovasc Surg. 2013;146:269-74. https://doi.org/10.1016/j.jtcvs. 2012.06.053
- Kaiser AD, Shad R, Hiesinger W, Marsden AL. A design-based model of the aortic valve for fluid-structure interaction. *Biomech Model Mechanobiol*. 2021; 20:2413-35. https://doi.org/10.1007/s10237-021-01516-7
- Kaiser AD, McQueen DM, Peskin CS. Modeling the mitral valve. Int J Numer Method Biomed Eng. 2019;35:e3240. https://doi.org/10.1002/cnm.3240
- Kaiser AD, Schiavone NK, Elkins CJ, McElhinney DB, Eaton JK, Marsden AL. Comparison of immersed boundary simulations of heart valve hemodynamics against in vitro 4D flow MRI data. *Ann Biomed Eng.* 2023;51:2267-88. https:// doi.org/10.1007/s10439-023-03266-2
- Yang W, Chan FP, Reddy VM, Marsden AL, Feinstein JA. Flow simulations and validation for the first cohort of patients undergoing the Y-graft Fontan procedure. J Thorac Cardiovasc Surg. 2015;149:247-55. https://doi.org/10.1016/j. jtcvs.2014.08.069
- Schwarz EL, Kelly JM, Blum KM, Hor KN, Yates AR, Zbinden JC, et al. Hemodynamic performance of tissue-engineered vascular grafts in Fontan patients. NPJ Regen Med. 2021;6:38. https://doi.org/10.1038/s41536-021-00148-w
- Matsushima S, Heß A, Lämmerzahl JR, Karliova I, Abdul-Khaliq H, Schäfers HJ. Unicuspid aortic valve repair with bicuspidization in the paediatric population. Eur J Cardiothorac Surg. 2021;59:253-61. https://doi.org/10.1093/ejcts/ezaa285
- Updegrove A, Wilson NM, Merkow J, Lan H, Marsden AL, Shadden SC. Sim-Vascular: an open source pipeline for cardiovascular simulation. *Ann Biomed Eng.* 2017;45:525-41. https://doi.org/10.1007/s10439-016-1762-8
- Peskin CS. Flow patterns around heart valves: a numerical method. *J Comput Phys.* 1972;10:252-71. https://doi.org/10.1016/0021-9991(72)90065-4
- Peskin CS. The immersed boundary method. Acta Numer. 2002;11:479-517. https://doi.org/10.1017/S0962492902000077
- Griffith BE, Hornung RD, McQueen DM, Peskin CS. An adaptive, formally second order accurate version of the immersed boundary method. *J Comput Phys*. 2007;223:10-49. https://doi.org/10.1016/j.jcp.2006.08.019
- Marom G, Haj-Ali R, Rosenfeld M, Schäfers HJ, Raanani E. Aortic root numeric model: annulus diameter prediction of effective height and coaptation in postaortic valve repair. *J Thorac Cardiovasc Surg.* 2013;145:406-11.e1. https://doi. org/10.1016/j.jtcvs.2012.01.080

Key Words: aortic valve repair, aortic valve simulations, bicuspidization

Kaiser et al Congenital

APPENDIX E1. SUPPLEMENTAL INFORMATION

Methods

Additional details on the methods are described as follows.

Construction of the model valves. The model valves were constructed via design-based elasticity, in which the closed configuration of the valve was designed via tuning parameters in a nonlinear partial differential equation. 12,13 This differential equation was derived from the requirement that tension in the valve leaflets supports a constant pressure load. The solution represented the predicted, loaded, closed configuration of the valve. From the closed configuration, a reference configuration and constitutive law for the leaflets were derived. Experimentally measured values of stretch (ratio of current length to reference length) were prescribed in the radial and circumferential directions, and then reference lengths were derived for the discretized model from these stretch ratios. E1 The shape of the stretch/tension response was exponential and zero at a stretch ratio of 1: the exponential rates were selected from experimental data. E2 The stiffnesses of the exponential responses locally were scaled to have tension needed by the predicted loaded configuration at the experimentally measured stretches. This completed the derivation of the reference configuration and constitutive law of the model valve.

To obtain an initial configuration suitable for fluidstructure interaction simulations, an ideal free edge configuration to reduce residual stress in the leaflets was computed algorithmically with an iterative search. This method searched for uniform stretch circumferentially and a specified prestretch along each (mathematical) fiber in the radial direction. First, a constant prestretch was prescribed to the radial direction fibers based on their predicted loaded stretch. An arbitrary curve of the form $a\sin^2\theta$ was computed from each of the commissures, where the optimal value of a was initially unknown. Each free edge point was then placed on a ray from the annulus to this curve at the prescribed distance from the annulus. The value of a was then optimized with MATLAB'S fsolve such the length of the resulting curve was approximately equal to the free edge rest length. This produced a configuration with the desired radial stretches and total free edge length, but without locally uniform stretch along the free edge. The following 2 steps were then repeated until the root mean squared difference of stretch along the free edge was less than 10^{-10} or after 2000 iterations. The free edge points were then distributed on a linear interpolant between the current points, spaced as a fraction of the rest length of each edge in the discretized model. To reobtain the prescribed radial stretch, each free edge point was again placed on a ray from the annulus at the required distance. In most cases, this process converged resulting in uniform stretches circumferentially on the free edge and the prescribed radial

prestretch. In some cases, the valve lacked sufficient circumferential or radial length for this process to converge and a nonuniform pattern of stretch occurred on the free edge. Nonetheless, running this algorithm still reduced the residual stretch and tension in the leaflets, and it was applied to all cases. This location was then fixed as a Dirichlet boundary condition, and a problem of mechanical equilibrium was solved with the reference configuration and constitutive law that was just derived with zero pressure loading. This process resulted in lower stretches throughout the valve. The leaflets were set to a thickness of 0.44 mm. E3 This configuration was then used as initial conditions for fluid-structure interaction simulations.

Construction of the model aorta. To construct the model aorta with SimVascular, a path line was selected that represented the approximate centerline of the vessel. Sim-Vascular then computed image slices normal to this path. The outer boundary of the lumen was manually segmented on these 2-dimensional segments from the left ventricular outflow tract through the distal ascending aorta. These 2-dimensional segmentations were lofted into a 3-dimensional surface representation, and a triangular mesh for this geometry was computed and exported for use in fluid-structure interaction simulations.

Flow extenders were added to the inlet and outlet of this geometry. The extender at the outlet was cylindrical and 1-cm long. The extender at the inlet was 3 cm in length; the first 1.5 cm constricts smoothly by 5 mm and is followed by 1.5 cm with a constant cross-sectional profile. Introducing this smooth constriction in the flow extender ensured numerical stability at the inlet during forward flow, and the flow averaging force of our previous work was omitted. The position was prescribed to be nearly rigid via stiff linear springs on the faces of the mesh and target points, stiff linear springs of zero rest length tied to a fixed location.

Fluid-structure interaction. The immersed boundary method used a regular Cartesian mesh to model the fluid, blood, whereas the structure, which includes the leaflet, scaffold on which the leaflets are mounted and model aorta was modeled as a continuum of mathematical fibers, which exert force along their axes. The fluid domain mesh occupied the entire region of interest, and the structure mesh occupied a proper subset of the fluid domain. At the interface of the fluid and structure, the meshes are not required to conform to each other. Coupling between the fluid and structure was handled via convolution with a discrete approximation to the Dirac delta function. These convolutions ensured that the structure moves with the fluid velocity, and force from the structure is appropriately distributed to the fluid. The use of nonconforming meshes allowed for fluid-structure interaction simulations with large elastic deformations of valve leaflets, rapid changes in the fluid domain geometry, and changes in the fluid domain

Congenital Kaiser et al

topology. Because of the diffuse interface coupling scheme, the structures such as leaflets interacted when they are a small but finite difference from each other, and no additional contact forces were required.^{E4}

All simulations were run with the open-source software package Immersed Boundary Adaptive Mesh Refinement (IBAMR).²¹ The spatial resolution was set to 0.5 mm for all simulations. In a convergence study in previous work, little difference was found between results with this resolution and 0.375 mm and concluded 0.5 mm was sufficient resolution. The time step was set to either $6 \cdot 10^{-6}$ or $5 \cdot 10^{-6}$ 10^{-6} s, the minimum that was found to be stable for each specific case. In previous work, little difference was found between the second cycle and third and fourth cycles. Thus, all cases were run for 2 cardiac cycles of 0.8 seconds duration, or 75 beats per minute. The first cycle was discarded due to initialization effects, and results from the second cycle are presented in this work. All simulations were run on 48 Intel Xeon Gold 5118 cores across 2 nodes with a 2.30 GHz clock speed via the Sherlock cluster at Stanford University.

Evaluation metrics. To evaluate regurgitation, the flow rates through the artery were computed by directly integrating the fluid velocity field at the inlet within IBAMR. To evaluate stenosis, the mean pressure was computed directly from the simulated fluid field. By using Paraview, the pressure was integrated over 2-dimensional slices in the left ventricular outflow tract and the STJ; the gradient reported was the difference of these 2 quantities. (Note that this was formally a pressure difference rather than a pressure gradient, but the term "pressure gradient" was used, as is standard in clinical practice.)

The orifice area during systole was computed as follows. A rigid body motion that maps the virtual basal ring to the unit circle was applied, and then each point of the valve was projected onto the plane of the virtual basal ring. Each point was then reflected over the unit circle and the outer boundary of these reflected points was computed via MATLAB'S boundary function. This produced a tight bounding polygon to this set of points. Using the original, rather than reflected, position of the points, this area of this polygon was approximately equal to the area internal to the valve.

Results

Three additional cases were run all with free edge length of approximately 1.6d in which the gross morphology varied in other ways. One case had less area or "bowl shape" to the leaflets, which created a more tube-like geometry with less leaflet material to billow. One case had less leaflet height, and 1 case had both less area and less height. These models were constructed to investigate the substantial variability in gross morphology that may occur even with consistent free edge length.

A visualization of 4 cases in systole and diastole showed subtle but substantial differences between cases, where the "standard" case used in Figure E1 was identical to the 1.57d case used throughout the main manuscript. With area removed, the systolic flow appeared qualitatively similar to the standard case. The systolic configuration of the leaflet appeared straighter and more cylindrical. In diastole, the valve appeared to be coapted below the free edge, and the free edge showed redundant length in this configuration. The case with height removed showed qualitatively similar flows and valve position to the standard case in both systole and diastole. The case with both height and area removed showed slightly stronger recirculation and cylinder-like shape during systole. In diastole, this case showed less billow height and billowed over a smaller portion of the leaflets.

Despite relatively similar performance, the scalar metrics still showed variation between cases (Table E1). The cases with reduced area showed modestly reduced orifice area and stroke volume and modestly increased pressure gradient, worse in the case that also had reduced leaflet height. These cases showed pressure gradients and stroke volume similar to those of the 1.4d case, despite having longer free edge lengths. In diastole, the cases with reduced height showed lower geometric height, as expected. Compared with cases with similar leaflet heights, the cases with reduced area showed reduced billow, increased effective height, effective height from minimum, effective height to geometric height ratio, and effective height from minimum to geometric height ratio. Thus, despite worse systolic performance, the cases with reduced area appeared to have a better diastolic configuration with less billow and better effective height.

These cases illustrated that the 3-dimensional geometry of the leaflets influenced billow and forward flow behaviors, even when 2 fundamental quantities that control leaflet size (free edge rest length and leaflet height) remained the same. Further, there appeared to be a consistent trade-off between systolic performance and the presence of billow and other poor diastolic behaviors. Experimental studies must be conducted to understand the clinical consequences of such changes.

E-References

- E1. Yap CH, Kim HS, Balachandran K, Weiler M, Haj-Ali R, Yoganathan AP. Dynamic deformation characteristics of porcine aortic valve leaflet under normal and hypertensive conditions. Am J Physiol Heart Circ Physiol. 2010;298: H395-405. https://doi.org/10.1152/ajpheart.00040.2009
- E2. May-Newman K, Lam C, Yin FCP. A hyperelastic constitutive law for aortic valve tissue. J Biomech Eng. 2009;131:1-7. https://doi.org/10.1115/1. 3127261
- E3. Sahasakul Y, Edwards WD, Naessens JM, Tajik AJ. Age-related changes in aortic and mitral valve thickness: implications for two-dimensional echocardiography based on an autopsy study of 200 normal human hearts. Am J Cardiol. 1988;62:424-30. https://doi.org/10.1016/0002-9149(88)90971-X
- E4. Lim S, Ferent A, Wang XS, Peskin CS. Dynamics of a closed rod with twist and bend in fluid. SIAM J Sci Comput. 2008;31:273-302. https://doi.org/10.1137/ 070699780

Kaiser et al Congenital

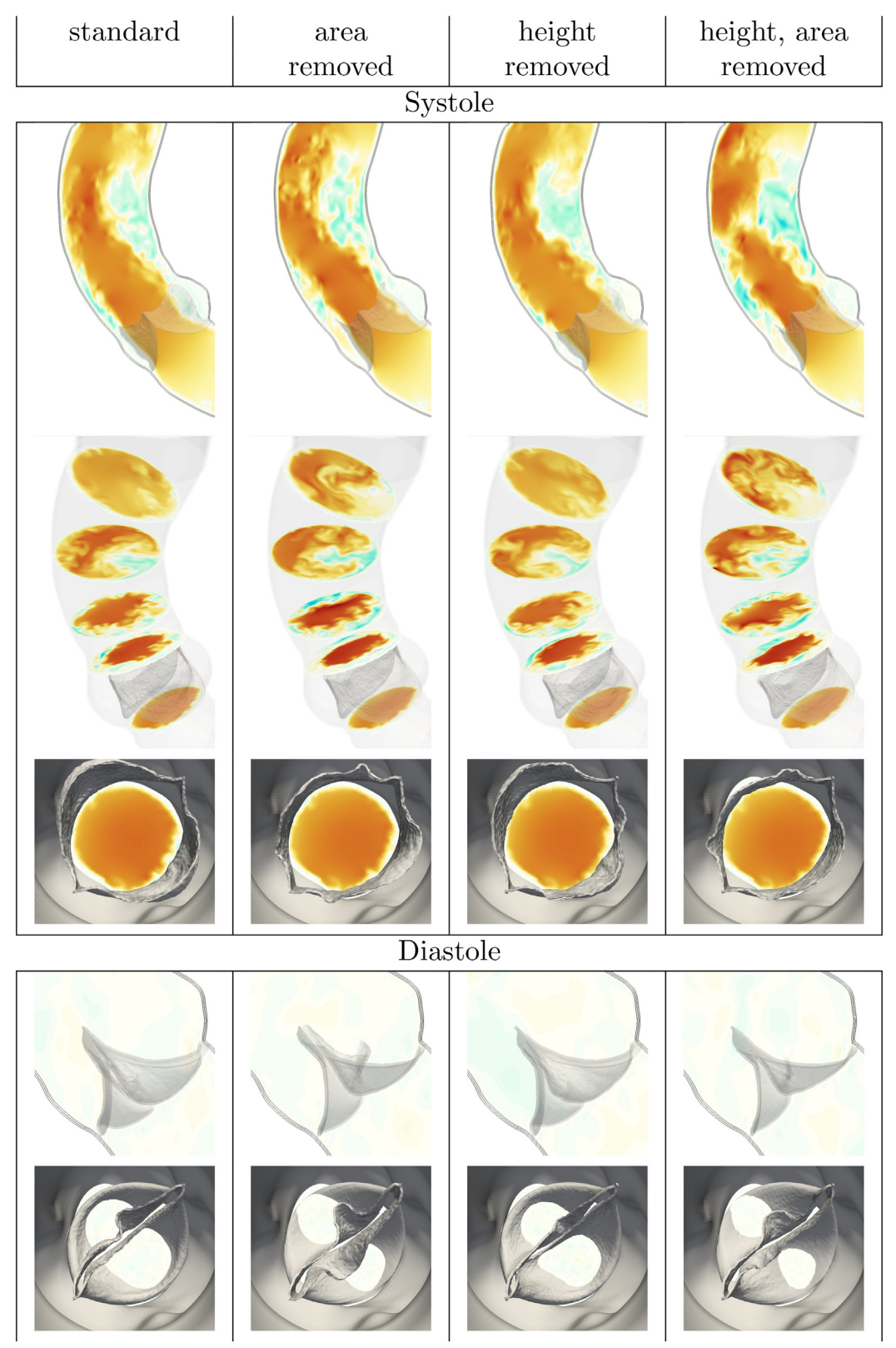


FIGURE E1. Comparison of variations in gross morphology with similar free edge lengths.

Congenital Kaiser et al

TABLE E1. Scalar metrics in systole and diastole

Systole									
Case	Orifice area (cm²)			Pressure gradient, mean (mm Hg)			Stroke volume (mL)		
Standard			3.45		6.92			75.52	
Less area	2.98			9.43			72.84		
Less height			3.27		7.31			75.23	
Less area, height			2.89		10.26			72.20	
				Diastole					
Case	G_h (cm)	G_h/r	Billow height (cm)	E_h (cm)	Eh,min (cm)	Eh/Gh	Eh,min/Gh	F (cm)	F/d
Standard	2.15	1.72	-0.28	0.59	0.87	0.27	0.40	4.02	1.61
Less area	2.22	1.78	-0.17	0.86	1.03	0.39	0.46	4.02	1.61
Less height	1.88	1.50	-0.23	0.30	0.54	0.16	0.29	4.29	1.71
Less area, height	1.94	1.55	-0.12	0.63	0.74	0.32	0.38	4.07	1.63

 G_h , Geometric height; r, annular radius; E_h , effective height; $E_{h,min}$, effective height from minimum height of valve taking billow into account; F, free edge length; d, annular